Annealing Controls Ultrafast Dynamics of Carrier Production in an OPV Incorporating a Non-fullerene Acceptor

Courtney A. DelPo[†], Sarah E. Bard[†], Gregory D. Scholes[†,*]

†Department of Chemistry, Princeton University, Princeton, New Jersey 08544, United States

AUTHOR INFORMATION

Corresponding Author

* Email: gscholes@princeton.edu

Abstract

Non-fullerene acceptors have emerged as leading candidates in organic photovoltaics pushing past some of the limitations of their fullerene counterparts with absorption extending in the visible and NIR, decreased air-sensitivity, and tunable energy levels. Significant progress has been made in demonstrating the potential of non-fullerene acceptor based devices to reach high efficiencies, however, a photophysical and mechanistic understanding of charge generation in these non-fullerene acceptors lags behind. In particular, the effects of annealing on carrier production have not been previously examined. Here, we use transient absorption spectroscopy and atomic force microscopy to examine the effect of solvent vapor annealing on a perylene diimide based non-fullerene acceptor, PDI-DPP-PDI. We find that when mixed with the donor PTB7-Th, the effect of solvent vapor annealing on PDI-DPP-PDI is to reduce geminate recombination leading to balanced exciton generation and charge separation.

TOC Graphics

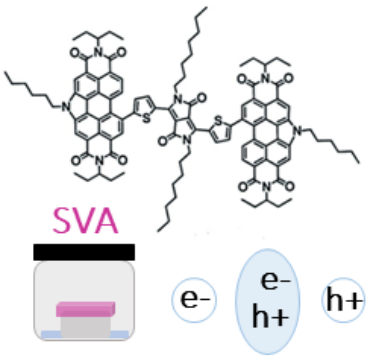

Keywords: Non-fullerene acceptors, organic photovoltaics, transient absorption spectroscopy, charge generation and separation, geminate recombination, solvent vapor annealing, thermal annealing

Introduction

As efforts towards the development of sustainable and renewable energy resources continue, organic solar cells offer great potential as a leading resource. In order to become competitive with commercialized silicon based solar cells, the power conversion efficiency (PCE), lifetime, and scalability of organic photovoltaics must first be improved.[1–5] Much of the previous research on the advancement of organic solar cells has focused on devices with fullerene-based acceptors which have high electron affinity and excellent morphology for charge separation and carrier transport.[6–10] However, fullerene-based acceptors have limited energy level tunability, low absorption in the visible and near infrared (NIR) regions, and air-sensitivity which restrict the possibility for further progress of device performance with fullerene-based devices.[11] In contrast, non-fullerene acceptors (NFAs) typically have greater absorption in the visible and NIR regions, can be air-stable, and have energy levels that are easily tunable through synthetic modification offering more opportunities for the enhancement of device performance and stability of organic solar cells.[12–16]

While the mechanisms behind charge generation and recombination and the corresponding relationship between these mechanisms, morphology, and device PCE are well documented for fullerene-based acceptors, the same foundational understanding remains lacking for NFAs deterring the progress of NFA devices. Concurrently, this foundational understanding of the operation of fullerene-based acceptors is not applicable to NFAs as a result of their differing properties.[17] In fullerene-based devices, the donor absorbs the majority of sunlight leading to a relatively straightforward charge generation process: a singlet exciton forms in the donor domain and diffuses to the donor-acceptor interface where electron transfer occurs to form a charge transfer (CT) intermediate that dissociates into free charges.[18] In contrast, as a result of their significant absorption in the visible and NIR, charge generation in NFAs includes a substantial contribution

of hole transfer from excitons formed in the acceptor domains. Unlike in fullerene-based acceptors, hole transfer in NFAs is dominated by a slow, exciton-diffusion mediated process. NFAs also have reported longer exciton diffusion lengths as compared to their fullerene-based counterparts.[19–21] One study found that trying to mimic the architecture of fullerene acceptors in the design of non-fullerene acceptors led to poor device efficiency further highlighting that the design principles of fullerene-based acceptors do not apply to NFAs.[22] While some studies have examined these types of effects arising from synthetically induced structural changes in NFAs,[23] notably, the mechanistic effects of annealing on NFAs have not been investigated.

Transient absorption is a well-suited tool to study the relationship between morphology and charge generation and recombination in NFAs because it has the ability to capture hole transfer with both selective pump excitation wavelengths and timescales covering tens to hundreds of picoseconds. While there has been excellent progress in improving the PCE of non-fullerene devices,[24–26] the progress in photophysical characterization lags behind hindering further improvement.[27] A combination of photophysical, morphological, and efficiency characterization offers the most complete picture to inform the design of future non-fullerene based devices. In this article, we use transient absorption spectroscopy and atomic force microscopy to examine the mechanism behind the improved PCE upon solvent vapor annealing (SVA) of the perylene diimide based non-fullerene acceptor, PDI-DPP-PDI (structure shown in Figure 1).

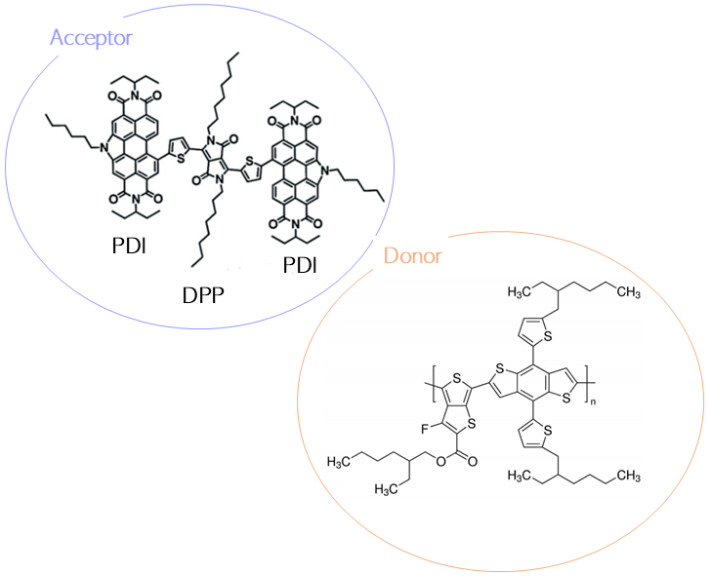

Figure 1. Structures of the acceptor (PDI-DPP-PDI) and donor (PTB7-Th) molecules used in this study.

McAfee et al. reported the synthesis of PDI-DPP-PDI and demonstrated that when blended in a device with the donor PTB7-Th (structure shown in Figure 1), the PCE of the device increased from 2.1% for the as-cast device to 5.0% for the SVA device with increased fill factor and short circuit current.[28] Contrary to other molecules, thermal annealing (TA) was observed to have a negligible effect on the morphology of this acceptor (Figure S1). Here, we examine the photophysics of the acceptor-only films and donor-acceptor blends under the two different annealing conditions (SVA and the control, TA) and demonstrate the central effect of annealing (SVA) is a reduction of geminate recombination and a corresponding balance between the amount of excitons reaching the donor-acceptor interface and the amount of excitons dissociating to charges at that interface with the new orientation of the acceptor molecule. In the TA blends, there is an imbalance of a large number of excitons reaching the interface, but only a fraction leading to the generation of charges.

Methods

PDI-DPP-PDI (perylene diimide flanked diketopyrrolopyrrole) and PTB7-Th (Poly([2,6′-4,8-di(5-ethylhexylthienyl)benzo[1,2-b;3,3-b]dithiophene]{3-fluoro-2[(2-ethylhexyl)carbonyl]thieno[3,4-b]thiophenediyl}) were purchased from Sigma Aldrich and used as received. Acceptor-only films of PDI-DPP-PDI were spin-coated from 7 mg/mL solutions in chloroform at 1500 RPM for 1 minute. Donor-acceptor blends were spin-coated from a total of ~12 mg/mL solutions in chloroform (ratio 60:40 PDI-DPP-PDI:PTB7-Th) at 1500 RPM for 1 minute. In the case of the solvent vapor annealing, substrates were placed in an enclosed jar and exposed to 0.5 mL of chloroform for 5-8 minutes. Absorption spectra were matched to the previously reported spectra upon solvent vapor annealing of PDI-DPP-PDI.[28] In the case of thermal annealing, substrates were heated on a hot-plate at 100°C for 5 minutes. Absorption measurements were conducted using a UV-Vis Cary 6000i Spectrometer. Fluorescence and quantum yield measurements were taken using a Horiba PTI QuantaMaster 400 Spectrofluorometer. Absolute fluorescence quantum yield measurements were taken using an integration sphere. A detailed description of the pump-probe setup used for the transient absorption measurements is provided elsewhere.[29] Briefly, a 1 kHz regeneratively amplified Ti:Sapphire laser (Coherent Libra) centered at 800 nm with a 45 fs pulse duration and 4 W of power is directed to a beam-splitter to produce the pump and probe arms. The reflected part of the light is directed into a commercial optical parametric amplifier (OPerA Solo) to produce the pump wavelengths used in this paper. The transmitted and reflected light are both directed into a commercial transient absorption spectrometer (Ultrafast Systems Helios) for the transient absorption measurements. The pump light is sent through a 500 Hz optical chopper before focusing on the sample. The probe pulse is generated by focusing the 800 nm light into a crystal specific for the white light or NIR probes used in this paper. All transient experiments were done at magic angle and with nitrogen

gas flowing over the samples. Phase and height images for the SVA film were obtained using a Bruker NanoMan Atomic Force Microscope. Because of the lower surface roughness of the TA film, the phase and height images for the TA film were obtained using the more sensitive Bruker Dimension ICON3 Atomic Force Microscope.

Results & Discussion

The absorbance maximum of PDI-DPP-PDI in the TA film is 530 nm with an additional peak at 500 nm and a broad shoulder centered around 650 nm (Figure 2a). The fluorescence of the TA film originates from the PDI excimer state and is broad and centered at 815 nm.[30] Upon SVA, the absorbance and fluorescence of the PDI-DPP-PDI (Figure 2) thin film changes. In the absorbance, a prominent new peak appears around 586 nm along with the presence of two peaks in the UV region around 350 nm and 370 nm. The appearance of the new peaks is also accompanied by a decrease in the absorbance of the peaks at 500 nm and 530 nm and an increase in absorbance of the peak at 300 nm (Figure 2a). These spectral changes indicate a change in the orientation of the molecule upon SVA that leads to a decreased PDI transition dipole and an increased DPP transition dipole. The new peaks at 586 nm, 350 nm, and 370 nm are attributed to DPP absorption.[31] The maximum fluorescence peak in the SVA film is 755 nm which is blue-shifted relative to that of the TA film at 815 nm (Figure 2b). The blue-shift and broadening of the fluorescence is also accompanied by an increase in the fluorescence quantum yield with excitation at 530 nm from 4.4% in the TA film to 17.3% in the SVA film.

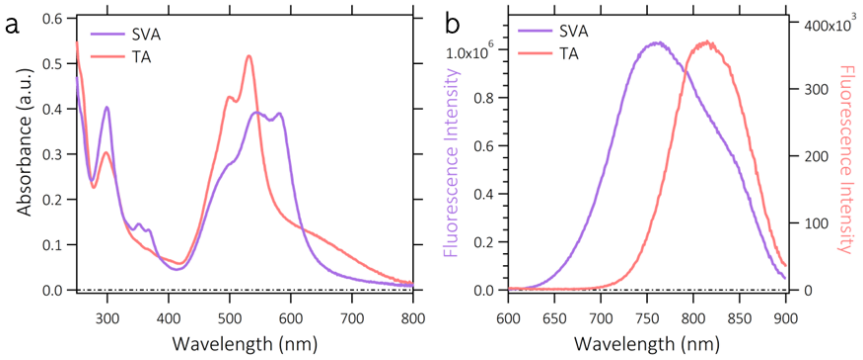

Figure 2. Absorption (a) and fluorescence (b) of PDI-DPP-PDI under the two different annealing conditions: SVA (solvent vapor annealing) and TA (thermal annealing). Fluorescence excitation wavelength is 530 nm.

The new orientation of the molecule upon SVA that leads to increased intensity of the DPP transitions in the steady-state absorption is supported by the excited-state spectra and dynamics which also demonstrate increased DPP contribution in the visible region. When exciting the acceptor-only films at 530 nm, the shape of the ground state bleach (GSB) in the visible region from 450 nm to 600 nm is consistent with the differences in the steady-state absorbance of the films under the different annealing conditions with increased intensity around 590 nm for the SVA film (Figure 3a,d). The GSB for the SVA film (Fig 3a, purple) features a spectral shape evolution in the duration of the experiment, while the GSB for the TA film does not (Figure 3d, red). In the region from 640 nm to 800 nm, both films feature a broad excited-state absorption (ESA, Figure 3b,e). As part of the ESA, the SVA film has an additional sharp peak feature at 780 nm which has been previously observed in the transient absorption spectra of DPP.[32] Consistent with the differences in spectral features, the dynamics across the visible region, shown through representative kinetic traces, vary for the SVA film (Figure 3c), but remain constant for the TA film (Figure 3f). This signals the contribution of multiple excited-state species to the features in the SVA film, but only one excited state species contributing to the features in the TA film. The

additional excited-state species contributing to the visible transient absorption features in the SVA film is DPP, which has a GSB in the same region.[32]

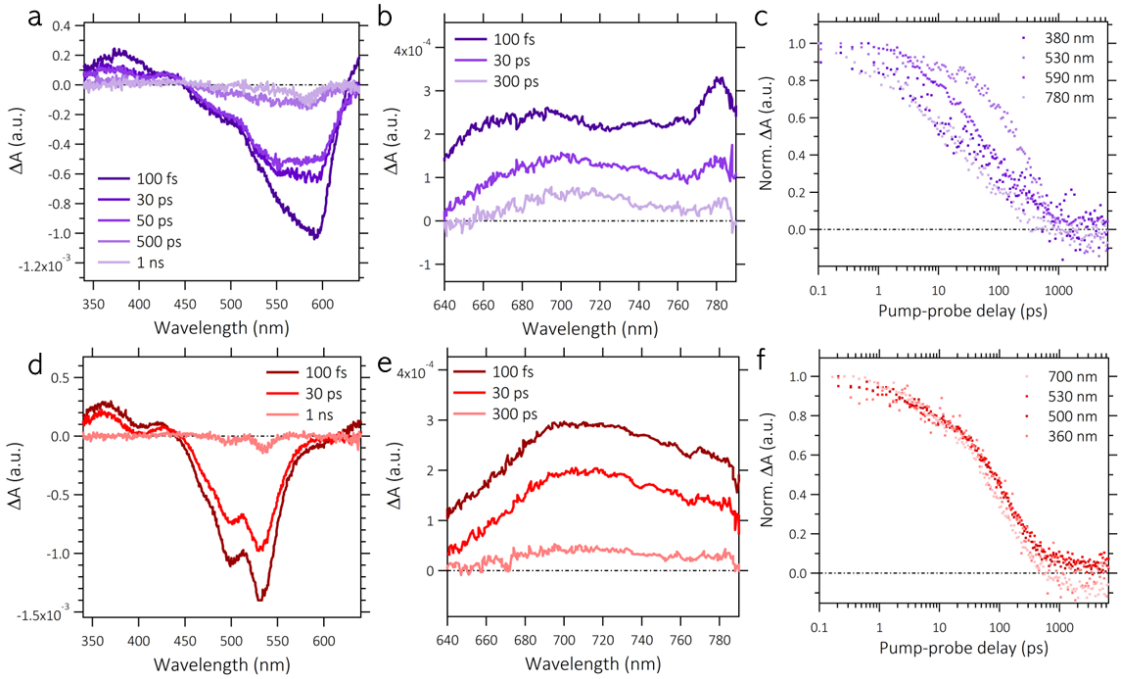

Figure 3. Visible transient absorption spectra (a-b, d-e) and selected kinetic traces (c, f) of the PDI-DPP-PDI films under the two annealing conditions: SVA (a-c, purple) and TA (d-f, red). Films were excited at 530 nm, 8 μJ/cm^2.

In contrast to the visible region where there are overlapping contributions from PDI and DPP, the NIR region has dominant features from PDI.[33] In particular, the ESA around 1300 nm (Figure 4a, c) has been previously attributed to a PDI excimer transition to a higher energy state with more charge transfer character.[30,34] The relative orientation of stacked PDI molecules and thus the electronic coupling between PDIs determines the energy, intensity, and rate of formation of the excimer state and corresponding dynamics of the ESA. In the SVA film, the ESA at 1300 nm rises with a time constant of ~19 ps which is about four times slower than the rise of the ESA in the TA film which has a time constant of ~5 ps (Figure 4b, d, Figures S2 and S3).[35] The slower rise dynamics in the SVA film point to reduced electronic coupling between PDI molecules in the excimer state. This is consistent with the greater red-shift and reduced fluorescence quantum yield

in the steady-state fluorescence of the TA film, which has stronger coupling and faster formation of the excimer state. The spectroscopic results we observe are consistent with a previous study on PDI excimers where excimer formation was compared in PDI dimers synthetically forced into a slip-stacked structure along the longitudinal axis to PDI dimers in a cofacial arrangement.[34] The slip-stacked formation led to higher fluorescence quantum yields, blue-shifted excimer fluorescence, and decreased rate of excimer formation. Because this is the same trend we observe in going from the TA films to the SVA films, the new orientation of the PDI molecule in this study upon SVA likely displaces the stacked PDIs along the longitudinal axis in a similar manner leading to the same observed reduction in electronic coupling. Because the excimer state can act as an exciton trap, the orientation of the molecule in the SVA film is expected to be better for device performance.[36]

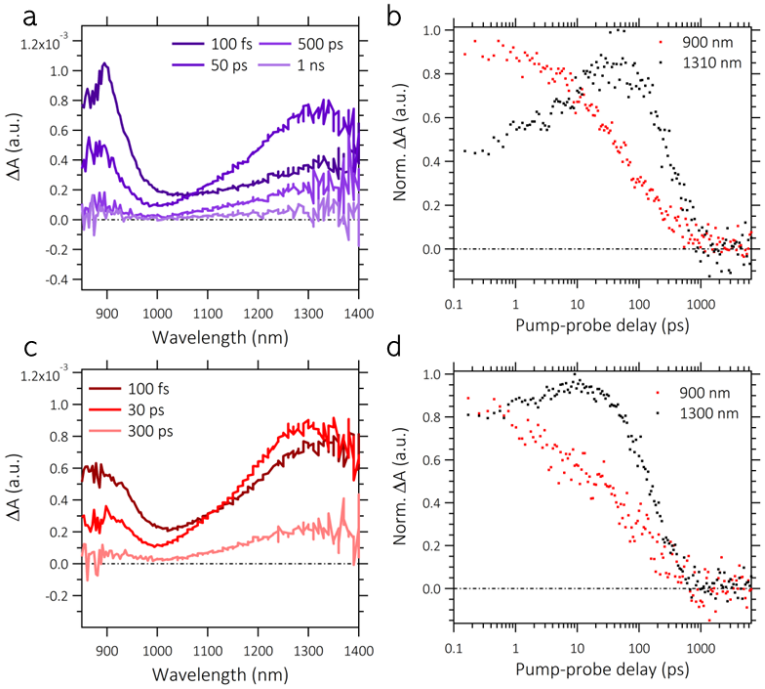

Figure 4. NIR transient absorption spectra (a, c) and selected kinetic traces (b, d) of the PDI-DPP-PDI films under the two annealing conditions: SVA (a, b) and TA (c, d). Films were excited at 530 nm, 8 μJ/cm^2.

To determine how the change in acceptor orientation upon SVA relates to the observed changes in device performance upon SVA, we studied the photophysics of blends of the PDI-DPP-PDI acceptor paired with the donor PTB7-Th under the two annealing conditions. The donor-acceptor ratio was selected to be the previously reported optimized donor-acceptor ratio for photovoltaic devices with this acceptor: 60:40 PTB7-Th:PDI-DPP-PDI.[28] When blended with the donor PTB7-Th, PDI-DPP-PDI exhibits the same changes in absorbance upon SVA that were seen with the acceptor-only films indicating the change in orientation upon SVA in the acceptor-only film is also present and significant in the blend (Figure 5a). The absorbance of the donor component in the SVA blend is slightly blue-shifted compared to the absorbance of the donor-only film (Figure S4). The fluorescence maximum of the SVA blend is again blue-shifted relative to that of the TA blend at 810 nm as compared to 845 nm. Under the same excitation conditions, the fluorescence of the TA blend is more intense than that of the SVA blend (Figure 4a, Figure S5). The fluorescence quantum yield of both the SVA and TA blends at primary excitation of either donor or acceptor is reduced to around 1%. The quenching of the fluorescence of the acceptor in the presence of the donor is more significant for the SVA blend than the TA blend. The decrease in fluorescence quantum yield from the SVA acceptor-only film to the SVA donor-acceptor blend (17.3% to 1%) was significantly greater than the corresponding decrease for the fluorescence quantum yield of the TA acceptor-only film to the TA donor-acceptor blend (4.4% to 1%).

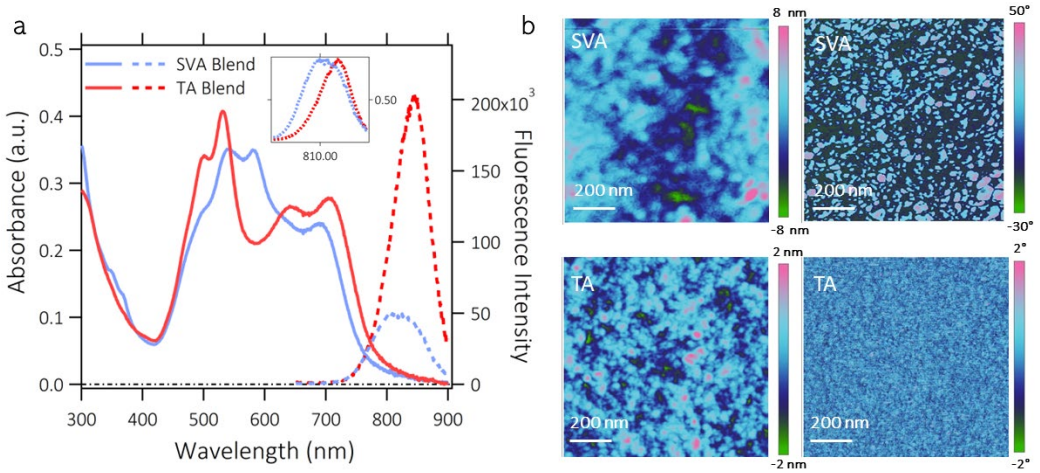

Figure 5. (a) Blend absorption (solid) and fluorescence (dotted, ex. 530 nm) for the films prepared with SVA (blue) and TA (red). Inset shows normalized blend fluorescence. (b) AFM height (left) and phase (right) images of the SVA (top) and TA (bottom) blends. Surface roughness for the SVA film was 2.4 nm and for the TA blend was 0.6 nm.

Atomic force microscopy (AFM) was used to probe the morphological differences of the blends under the two annealing conditions. The AFM height and phase images reveal the presence of qualitatively larger domains in the SVA film (Figure 5b top) as compared to the TA film (Figure 5b bottom). The TA film appears to have a more finely intermixed blend of donor and acceptor domains. The SVA film also shows the presence of small aggregates with a larger surface roughness (~2.4 nm) than the TA film (surface roughness ~0.6 nm). The surface roughness of the SVA blend is consistent with previous reports.[28] The new orientation of the acceptor molecule upon SVA that led to the spectroscopic differences shown in Figures 2-5 also leads to the formation of the larger domains in the blend. These morphological differences lead to differences in charge generation and recombination which will be revealed in the transient absorption studies.

Transient absorption spectroscopy was performed in the visible and the NIR regions with selective excitation of the donor and the acceptor in both the SVA and TA blends. Because NFAs absorb in the visible region (unlike their fullerene counterparts), hole-transfer from the acceptor to the donor is a significant process in determining overall device efficiency and it is therefore

important to study how the dynamics and spectral features change with excitation of the donor versus excitation of the acceptor under the two annealing conditions. We begin here with primary excitation of the donor (excitation 710 nm). In both the SVA (blue) and TA (red) blends, the GSB (Figure 6a-b) features a dominant contribution from the donor (Figure S6). In the NIR (Figure 6d-e), there are two features of interest also from the donor: the donor polaron feature (P^+) and the donor singlet exciton feature (Ex). Both of these features have been previously assigned in a blend with the same donor, PTB7-Th, but other acceptors.[22] The donor polaron signal is unique to the blend while the Ex feature is present in the donor-only film spectra (Figure S6). Furthermore, the donor polaron signal is indicative of the formation of free charges on the donor while the decay of the Ex feature is associated with exciton transport from the donor domain to the interface. In the SVA blend, there is a greater Ex signal present at early times (Figure 6d) and a corresponding slower decay of this Ex feature (Figure 6f) with an initial time constant of approximately 2.5 ps as compared to the TA blend with an Ex decay initial time constant of approximately 700 fs (Figures S7 and S8). At the earliest timescales before charge transfer has occurred and with primary excitation of the donor, the main contributor to the GSB is also the donor exciton signal. Consistent with the time constants for the NIR Ex feature, the initial time constant of the decay of the donor GSB feature in the SVA blend is slower at about 1.5 ps as compared to the TA blend GSB with an initial time constant of around 300 fs (Figure 6c, Figures S9 and S10). These observations are also supported by the AFM images that reveal the TA blend has small intermixed domains which leads to faster exciton arrival at the interface and consequently a larger number of excitons reaching the interface. The magnitude and dynamics of the donor polaron signal are comparable in both the TA and SVA blends (Figure 6d-f) indicating a similar quantity of charge

generation in both blends with excitation of the donor despite the slower exciton arrival at the interface in the SVA blend.

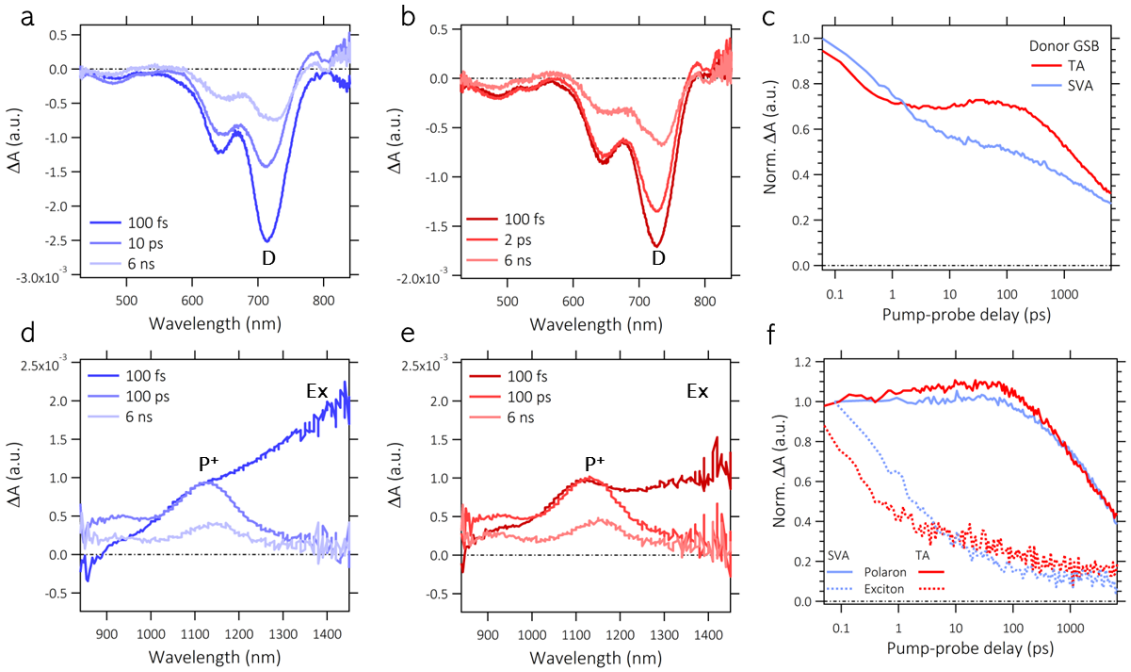

Figure 6. Transient absorption spectra and dynamics of the SVA (blue) and TA (red) blends when exciting the donor (710 nm, 4 μJ/cm^2). D is the donor bleach, Ex is the donor singlet exciton, P^+ is the donor polaron signal.

We now transition to excitation of the acceptor in the blends. In the visible region, we observe hole-transfer through a rise in the signal of the bleach of the donor and a concomitant decay of the bleach of the acceptor (Figure 7a-b, indicated with arrows) for both the TA and SVA blends. In blends with NFAs, hole-transfer has been demonstrated to be a biphasic process with an ultrafast interfacial component followed by a dominant slow but efficient diffusion-mediated component on the timescale of hundreds of picoseconds.[27,37–40] Here, we observe this dominant slow and efficient hole-transfer in the GSB dynamics of both the TA and SVA blends (Figure 7e). The larger rise in the donor GSB signal in the TA blend signals greater hole-transfer efficiency (Figure 7b, e). However, the donor GSB signal contains all of the products of charge transfer which include both separated charges and bound charge transfer (CT) excitons.[41] As a result, the

increased hole transfer efficiency does not necessarily lead to greater free charge generation and device performance as we know the TA photovoltaic device has been reported to have poorer device performance as compared the SVA device. To probe the generation of free charges without the other products of charge transfer, we monitor the donor polaron signal in the NIR (Fig. 7c,d). The large discrepancy in the signal intensities of the donor GSB and the donor polaron for the TA blend (Figure 7e, red) is an indication of geminate recombination where bound CT excitons contributing to the donor GSB recombine instead of separating into free charges. By comparing the signal intensities at their peaks, the donor polaron signal and indicator of free charge generation constitutes only 33% of the signal of all products of charge transfer in the TA blend. In contrast, in the SVA blend, the donor GSB signal (Figure 7e, blue) is equal in magnitude to the donor polaron signal indicating the hole transfer leads directly to the generation of free charges with reduced geminate recombination. The balanced exciton generation and charge separation observed in the transient dynamics of the SVA blend and absent in the dynamics of the TA blend is a contributing factor to the observed increase in device performance with SVA. The results of this paper are summarized in Scheme 1 below.

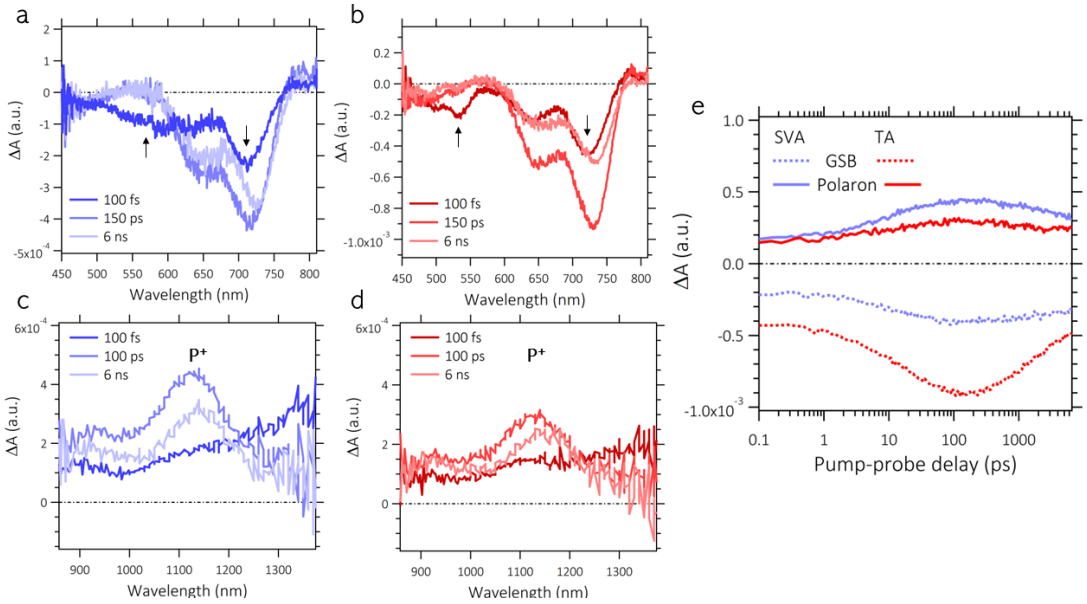

Figure 7. Transient absorption spectra and selected dynamics of the SVA (blue) and TA (red) blends when exciting the acceptor (530 nm, 4 μJ/cm^2).

Conclusion

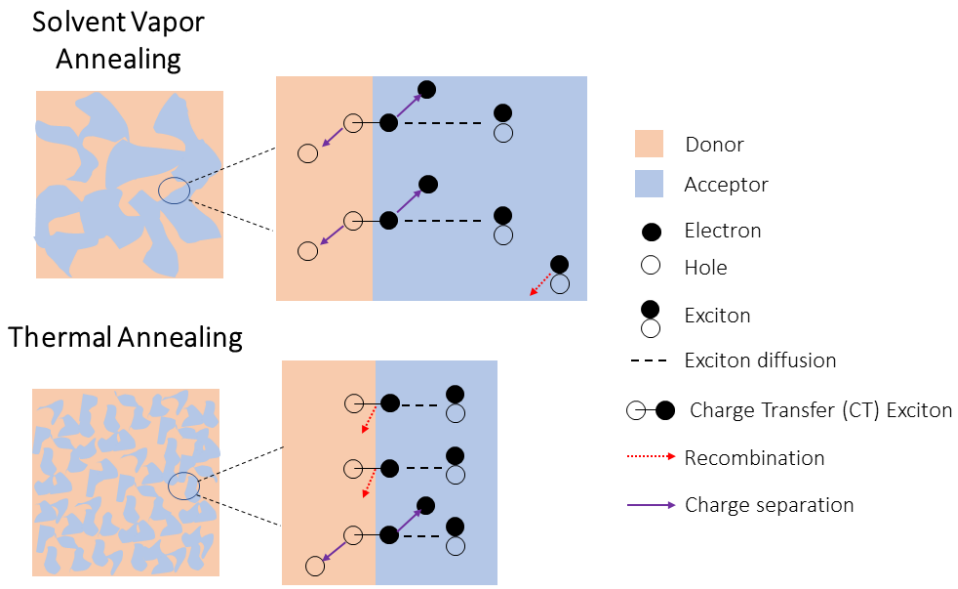

Scheme 1. Pictorial summary of the results of the paper. The changes in the geometry of the acceptor molecule upon SVA, as confirmed in the spectroscopy on the acceptor-only films, leads to the formation of larger acceptor domains in the SVA donor-acceptor blends (evidenced by the larger blue domains in the film and close-up of the interface above). The larger domains lead to longer distances for excitons to reach the donor-acceptor interface and a reduced number of excitons thus reaching the interface. However, excitons that reach the interface generate charges through charge separation. In contrast, in the TA film, a greater number of excitons reach the interface, however, at the interface, excitons are more likely to recombine than to separate and form free charges.

The spectroscopic characterization of the acceptor-only and donor-acceptor blend films reveals a complex picture of why the PCE of devices with PDI-DPP-PDI is increased upon SVA. The spectroscopy on the acceptor-only films indicated a new orientation of the molecule with SVA that led to a more prominent DPP contribution and reduced electronic coupling between PDIs on stacked molecules. The new orientation was also present in the SVA blends and is favorable for reducing recombination in a device. In the blends, TA leads to better miscibility and smaller size of donor and acceptor domains (Figure 5b) which we have demonstrated leads to the positive

characteristics of faster exciton arrival at the charge-generating donor-acceptor interface (Figure 6 and 7) and greater hole transfer efficiency (Figure 7b, e) as compared to the SVA blends. However, the orientation of the molecules in the TA blend film leads to the detrimental effects of greater recombination as evidenced by the stronger fluorescence (Figure 5a) and reduced free charge generation (Figure 7e). Using several spectroscopic techniques, including transient absorption spectroscopy, we were able to present a complete analysis of the effects of annealing on device performance in organic photovoltaics with PDI-DPP-PDI. Specifically, the effect of SVA is to engineer a more favorable orientation of the acceptor molecule that leads to balanced exciton and charge generation with reduced geminate recombination.

ASSOCIATED CONTENT

Supporting Information.

The following files are available free of charge.

Comparison of TA and as-cast films, global analysis results for the NIR time constants, donor absorption and fluorescence, fluorescence excitation spectra, donor transient absorption spectra, global analysis results for the SVA and TA blends

AUTHOR INFORMATION

Notes

The authors declare no competing financial interests.

ACKNOWLEDGMENT

This research is funded by the U.S. Department of Energy, Office of Science, Office of Basic Energy Sciences Solar Photochemistry program, under Award Number DE-SC0015429. C.A.D.

acknowledges the use of Princeton's Imaging and Analysis Center, which is partially supported by the Princeton Center for Complex Materials, a National Science Foundation (NSF)-MRSEC program (DMR-1420541). We acknowledge Guangming Cheng for assistance with the AFM measurements and Gregory Welch for providing valuable information on the solvent vapor annealing process.

References

(1) Riede, M.; Spoltore, D.; Leo, K. Organic Solar Cells—The Path to Commercial Success. *Advanced Energy Materials* **2021**, *11* (1), 2002653
(2) Chauhan, A. K.; Jha, P.; Aswal, D. K.; Yakhmi, J. V. Organic Devices: Fabrication, Applications, and Challenges. *J. Electron. Mater.* **2022**, *51* (2), 447–485
(3) Duan, L.; Uddin, A. Progress in Stability of Organic Solar Cells. *Adv. Sci.* **2020**, *7* (11), 1903259
(4) Cheng, P.; Zhan, X. Stability of Organic Solar Cells: Challenges and Strategies. *Chem. Soc. Rev.* **2016**, *45* (9), 2544–2582
(5) Elumalai, N. K.; Uddin, A. Open Circuit Voltage of Organic Solar Cells: An in-Depth Review. *Energy Environ. Sci.* **2016**, *9* (2), 391–410
(6) Zhan, C.; Zhang, X.; Yao, J. New Advances in Non-Fullerene Acceptor Based Organic Solar Cells. *RSC Adv.* **2015**, *5* (113), 93002–93026
(7) Vandewal, K.; Tvingstedt, K.; Gadisa, A.; Inganäs, O.; Manca, J. V. On the Origin of the Open-Circuit Voltage of Polymer–Fullerene Solar Cells. *Nature Mater* **2009**, *8* (11), 904–909
(8) Koster, L. J. A.; Mihailetchi, V. D.; Ramaker, R.; Blom, P. W. M. Light Intensity Dependence of Open-Circuit Voltage of Polymer:Fullerene Solar Cells. *Appl. Phys. Lett.* **2005**, *86* (12), 123509
(9) Thompson, B. C.; Fréchet, J. M. J. Polymer–Fullerene Composite Solar Cells. *Angew. Chem. Int. Ed.* **2008**, *47* (1), 58–77
(10) Khlyabich, P. P.; Burkhart, B.; Rudenko, A. E.; Thompson, B. C. Optimization and Simplification of Polymer–Fullerene Solar Cells through Polymer and Active Layer Design. *Polymer* **2013**, *54* (20), 5267–5298
(11) Chen, W.; Zhang, Q. Recent Progress in Non-Fullerene Small Molecule Acceptors in Organic Solar Cells (OSCs). *J. Mater. Chem. C* **2017**, *5* (6), 1275–1302
(12) Lopez, S. A.; Sanchez-Lengeling, B.; de Goes Soares, J.; Aspuru-Guzik, A. Design Principles and Top Non-Fullerene Acceptor Candidates for Organic Photovoltaics. *Joule* **2017**, *1* (4), 857–870
(13) Zhang, G.; Zhao, J.; Chow, P. C. Y.; Jiang, K.; Zhang, J.; Zhu, Z.; Zhang, J.; Huang, F.; Yan, H. Nonfullerene Acceptor Molecules for Bulk Heterojunction Organic Solar Cells. *Chem. Rev.* **2018**, *118* (7), 3447–3507
(14) McAfee, S. M.; Payne, A.-J.; Dayneko, S. V.; Kini, G. P.; Song, C. E.; Lee, J.-C.; Welch, G. C. A Non-Fullerene Acceptor with a Diagnostic Morphological Handle for Streamlined

Screening of Donor Materials in Organic Solar Cells. *J. Mater. Chem. A* **2017**, *5* (32), 16907–16913
(15) Ye, L. et al. Unraveling the Influence of Non-Fullerene Acceptor Molecular Packing on Photovoltaic Performance of Organic Solar Cells. *Nat Commun* **2020**, *11* (1), 6005
(16) Sharma, V.; Koenig, J. D. B.; Welch, G. C. Perylene Diimide Based Non-Fullerene Acceptors: Top Performers and an Emerging Class Featuring N-Annulation. *J. Mater. Chem. A* **2021**, *9* (11), 6775–6789
(17) Greenstein, B. L.; Hutchison, G. R. Organic Photovoltaic Efficiency Predictor: Data-Driven Models for Non-Fullerene Acceptor Organic Solar Cells. *J. Phys. Chem. Lett.* **2022**, *13* (19), 4235–4243
(18) Pugliese, S. N.; Gallaher, J. K.; Uddin, M. A.; Ryu, H. S.; Woo, H. Y.; Hodgkiss, J. M. Spectroscopic Comparison of Charge Dynamics in Fullerene and Non-Fullerene Acceptor-Based Organic Photovoltaic Cells. *J. Mater. Chem. C* **2022**, *10* (3), 908–920
(19) Firdaus, Y. et al. Long-Range Exciton Diffusion in Molecular Non-Fullerene Acceptors. *Nat Commun* **2020**, *11* (1), 5220
(20) Hume, P. A.; Jiao, W.; Hodgkiss, J. M. Long-Range Exciton Diffusion in a Non-Fullerene Acceptor: Approaching the Incoherent Limit. *J. Mater. Chem. C* **2021**, *9* (4), 1419–1428
(21) Chandrabose, S. et al. High Exciton Diffusion Coefficients in Fused Ring Electron Acceptor Films. *J. Am. Chem. Soc.* **2019**, *141* (17), 6922–6929
(22) Yi, X. et al. Impact of Nonfullerene Molecular Architecture on Charge Generation, Transport, and Morphology in PTB7-Th-Based Organic Solar Cells. *Adv. Funct. Mater.* **2018**, *28* (32), 1802702
(23) Liu, Z.; Zhang, L.; Shao, M.; Wu, Y.; Zeng, D.; Cai, X.; Duan, J.; Zhang, X.; Gao, X. Fine-Tuning the Quasi-3D Geometry: Enabling Efficient Nonfullerene Organic Solar Cells Based on Perylene Diimides. *ACS Appl. Mater. Interfaces* **2018**, *10* (1), 762–768
(24) Karki, A.; Gillett, A. J.; Friend, R. H.; Nguyen, T. The Path to 20% Power Conversion Efficiencies in Nonfullerene Acceptor Organic Solar Cells. *Adv. Energy Mater.* **2021**, *11* (15), 2003441
(25) Wang, Y.; Lee, J.; Hou, X.; Labanti, C.; Yan, J.; Mazzolini, E.; Parhar, A.; Nelson, J.; Kim, J.; Li, Z. Recent Progress and Challenges toward Highly Stable Nonfullerene Acceptor-Based Organic Solar Cells. *Adv. Energy Mater.* **2021**, *11* (5), 2003002
(26) Xiong, J.; Xu, J.; Jiang, Y.; Xiao, Z.; Bao, Q.; Hao, F.; Feng, Y.; Zhang, B.; Jin, Z.; Ding, L. Fused-Ring Bislactone Building Blocks for Polymer Donors. *Science Bulletin* **2020**, *65* (21), 1792–1795
(27) Chen, Z.; Zhu, H. Photoinduced Charge Transfer and Recombination Dynamics in Star Nonfullerene Organic Solar Cells. *J. Phys. Chem. Lett.* **2022**, *13* (4), 1123–1130
(28) McAfee, S. M.; Dayneko, S. V.; Josse, P.; Blanchard, P.; Cabanetos, C.; Welch, G. C. Simply Complex: The Efficient Synthesis of an Intricate Molecular Acceptor for High-Performance Air-Processed and Air-Tested Fullerene-Free Organic Solar Cells. *Chem. Mater.* **2017**, *29* (3), 1309–1314
(29) Pensack, R. D.; Ostroumov, E. E.; Tilley, A. J.; Mazza, S.; Grieco, C.; Thorley, K. J.; Asbury, J. B.; Seferos, D. S.; Anthony, J. E.; Scholes, G. D. Observation of Two Triplet-Pair Intermediates in Singlet Exciton Fission. *J. Phys. Chem. Lett.* **2016**, *7* (13), 2370–2375
(30) Brown, K. E.; Salamant, W. A.; Shoer, L. E.; Young, R. M.; Wasielewski, M. R. Direct Observation of Ultrafast Excimer Formation in Covalent Perylenediimide Dimers Using

Near-Infrared Transient Absorption Spectroscopy. *J. Phys. Chem. Lett.* **2014**, *5* (15), 2588–2593
(31) Dhar, J.; Venkatramaiah, N.; A., A.; Patil, S. Photophysical, Electrochemical and Solid State Properties of Diketopyrrolopyrrole Based Molecular Materials: Importance of the Donor Group. *J. Mater. Chem. C* **2014**, *2* (17), 3457–3466
(32) Popli, C.; Jang, Y.; Patil, Y.; Misra, R.; D'Souza, F. Formation of Highly Efficient, Long-Lived Charge Separated States in Star-Shaped Ferrocene-Diketopyrrolopyrrole-Triphenylamine Donor–Acceptor–Donor Conjugates. *Chem. Eur. J.* **2020**, *26* (66), 15109–15115
(33) Mauck, C. M.; Bae, Y. J.; Chen, M.; Powers-Riggs, N.; Wu, Y.; Wasielewski, M. R. Charge-Transfer Character in a Covalent Diketopyrrolopyrrole Dimer: Implications for Singlet Fission. *ChemPhotoChem* **2018**, *2* (3), 223–233
(34) Margulies, E. A.; Shoer, L. E.; Eaton, S. W.; Wasielewski, M. R. Excimer Formation in Cofacial and Slip-Stacked Perylene-3,4:9,10-Bis(Dicarboximide) Dimers on a Redox-Inactive Triptycene Scaffold. *Phys. Chem. Chem. Phys.* **2014**, *16* (43), 23735–23742
(35) Snellenburg, J. J.; Laptenok, S. P.; Seger, R.; Mullen, K. M.; Stokkum, I. H. M. van. **Glotaran** : A *Java* -Based Graphical User Interface for the *R* Package **TIMP**. *J. Stat. Soft.* **2012**, *49* (3), 1-22
(36) Hartnett, P. E. et al., T. J. Slip-Stacked Perylenediimides as an Alternative Strategy for High Efficiency Nonfullerene Acceptors in Organic Photovoltaics. *J. Am. Chem. Soc.* **2014**, *136* (46), 16345–16356
(37) Yao, N. et al. Efficient Charge Transport Enables High Efficiency in Dilute Donor Organic Solar Cells. *J. Phys. Chem. Lett.* **2021**, *12* (20), 5039–5044
(38) Chen, Z.; Chen, X.; Qiu, B.; Zhou, G.; Jia, Z.; Tao, W.; Li, Y.; Yang, Y. M.; Zhu, H. Ultrafast Hole Transfer and Carrier Transport Controlled by Nanoscale-Phase Morphology in Nonfullerene Organic Solar Cells. *J. Phys. Chem. Lett.* **2020**, *11* (9), 3226–3233
(39) Wen, T. et al. Simple Non-Fused Electron Acceptors Leading to Efficient Organic Photovoltaics. *Angew. Chem. Int. Ed.* **2021**, *60* (23), 12964–12970
(40) Wu, Q.; Wang, W.; Wu, Y.; Chen, Z.; Guo, J.; Sun, R.; Guo, J.; Yang, Y. (Michael); Min, J. High-Performance All-Polymer Solar Cells with a Pseudo-Bilayer Configuration Enabled by a Stepwise Optimization Strategy. *Adv. Funct. Mater.* **2021**, *31* (15), 2010411
(41) Zhou, G. et al. Marcus Hole Transfer Governs Charge Generation and Device Operation in Nonfullerene Organic Solar Cells. *ACS Energy Lett.* **2021**, *6* (8), 2971–2981